Special Issue: MDA2018

Institution of MECHANICAL ENGINEERS
Journal of MATERIALS: DESIGN AND APPLICATIONS

Proc IMechE Part L:
J Materials: Design and Applications
0(0) 1–8

DOI: 10.1177/1464420718809133
journals.sagepub.com/home/pil
SAGE

Ultrasonic spot welding of dissimilar 2024Al alloy and SiCp/2009Al composite

VK Patel[1], SD Bhole[1], DL Chen[1], DR Ni[2], BL Xiao[2] and ZY Ma[2]

Abstract

Dissimilar welding of 2024Al alloy to SiC/2009Al composite was conducted via solid-state ultrasonic spot welding technique. Defect-free sound spot welds were successfully achieved. SiCp particles were observed to migrate from the composite side to 2024Al side along with the interfacial interlocking during the intense high-frequency rubbing, which increased with increasing welding energy. The microhardness across the ultrasonic spot welded similar and dissimilar joints remained nearly constant. The tensile lap shear failure load increased with increasing welding energy, and satisfied the requirements of AWS standard D17.2 for spot welding. In addition to room temperature tensile lap shear tests, all the similar and dissimilar joints were subjected to tensile tests at varying temperatures and their respective results were discussed.

Keywords

Aluminum alloy, metal matrix composite, ultrasonic spot welding, tensile lap shear test, microhardness

Date received: 2 August 2018; accepted: 4 October 2018

Introduction

Lightweighting has been considered as one of the most effective methods to improve fuel efficiency and reduce climate-changing, environment-damaging, and human death-causing[a] emissions in the automotive and aerospace industries.[1–4] Aluminum alloys are thus being considered for the fabrication of vehicles due to its low density, superior formability, and excellent corrosion resistance.[5,6] However, they have relatively lower mechanical properties in comparison with advanced high-strength steels. As a result, efforts have been made to improve the mechanical properties of Al alloys via addition of particle reinforcements.[7,8] SiC particles (SiCp) reinforced aluminum matrix composites (AMCs) have been of great interest because of high specific stiffness, high strength, excellent wear resistance, superior fatigue strength, high formability, and attractive thermal and electrical characteristics.[9,10] The lightweighting structural applications of aluminum alloys and their composites inevitably involve welding and joining, especially dissimilar welding. It is difficult to achieve defect-free welds using conventional fusion welding techniques due to the occurrence of segregation and deleterious reactions between the reinforcement particles and liquid aluminum in the fusion zone.[9] Furthermore, the porosity in the fusion zone, development of Al–C intermetallic phase and incomplete mixing of parent and filler materials also limit the application of fusion welding. Thus, there is an urgent need to develop an alternative method to join aluminum alloys and their composites. In this case the solid-state welding methods would be desirable.[11]

Recently friction stir welding (FSW) has been widely used to join AMCs in the aerospace and automobile industries for thinner and thicker gage sheet.[11,12] These studies have indicated that high-quality FSW composite joints could be achieved using optimized parameters. However, to the best of the authors' knowledge, the joining of AMCs in the form of spot geometry as a friction stir spot welding (FSSW) has not been limited. The relatively longer welding time, the presence of exit hole after welding and the relatively high-energy consumption would be the limiting factors for the widespread adoption of

[1]Department of Mechanical and Industrial Engineering, Ryerson University, Toronto, ON, Canada
[2]Shenyang National Laboratory for Materials Science, Institute of Metal Research, Chinese Academy of Sciences, Shenyang, China

Corresponding authors:
DL Chen, Department of Mechanical and Industrial Engineering, Ryerson University, 350 Victoria Street, Toronto, ON M5B 2K3, Canada.
Email: dchen@ryerson.ca
ZY Ma, Shenyang National Laboratory for Materials Science, Institute of Metal Research, Chinese Academy of Sciences, Shenyang, China.
Email: zyma@imr.ac.cn

FSSW in the automotive and aerospace manufacturing. An alternate solid-state spot welding technique, ultrasonic spot welding (USW), has recently gained more attention since it is considered as an emerging technology for joining lightweight alloys.[13–15] In USW, the coalescence is generated via a simultaneous application of localized high-frequency vibratory energy and moderate clamping forces.[16] Our previous study[17] showed that USW was able to produce a sound joint between similar AMC sheets. It is unknown if aluminum alloy and AMC can be properly welded via USW. The objective of this study was, therefore, to explore the feasibility of welding 2024Al alloy and SiCp/2009 composite and examine the microstructure and mechanical properties of such USWed dissimilar joints at varying temperatures.

Materials and experimental procedure

In the present work, 1.5-mm-thick as-rolled sheets of 2024Al alloy (composition in wt%: 3.8–4.9Cu, 1.2–1.8Mg, 0.3–0.9Mn, 0.5Si, 0.5Fe, 0.1Cr, and balance Al) and SiCp/2009Al composite (composition in wt%: 4.0Cu, 1.5Mg, and balance Al with 17 vol.% SiC particles) in T6 condition were used for USW. For the SiCp/2009Al composite (where a hot pressed ingot was first extruded and subsequently rolled into 1.5 mm thick sheet), SiC particles with an average size of 7 µm were adopted as reinforcements. The small sheets/workpieces of 80 mm long and 15 mm wide were sheared, with the faying surfaces ground using 120 emery paper, and then washed using acetone followed by ethanol and dried before welding. The welding was performed at the center of an overlapped area of 20 mm long in the length direction of workpieces with a dual wedge-reed Sonobond-MH2016 HP-USW system. A schematic diagram of USW process is shown in Figure 1, where an image of sonotrode tip is inserted to indicate the sonotrode tip tooth orientation with respect to the ultrasonic vibration direction. The samples were welded at a welding energy ranging from 500 to 3000 J at a constant power setting of 2000 W, an impedance setting of 8 (N s)/m and a pressure of 0.414 MPa. To achieve 500 to 3000 J energy inputs, the USW procedure took 0.25 to 1.5 s. Cross-sectional samples for scanning electron microscopy (SEM) were polished using diamond paste and MasterPrep. X-ray diffraction (XRD) was carried out on fracture surfaces after tensile lap shear tests, using CuK_{α} radiation at 45 kV and 40 mA. The diffraction angle (2θ) at which the X-rays hit the samples varied from 20° to 100° with a step size of 0.05° and 2 s in each step. A computerized Buehler Vickers microhardness testing machine was used for the microhardness tests diagonally across the welded joints using a load of 500 g for 15 s. The distance between two successive microhardness measurement was 0.5 mm. Microhardness tests were conducted according to ASTM standard (ASTM E384-17). Tensile lap shear tests of the welds were conducted to measure the failure load using a fully computerized united testing machine with a constant crosshead speed of 1 mm/min in air at low (-40 °C), room, and high (180 °C) temperature environments. In the tensile lap shear testing, restraining shims or spacers were used to minimize the rotation of the joints and maintain the shear loading as long as possible.

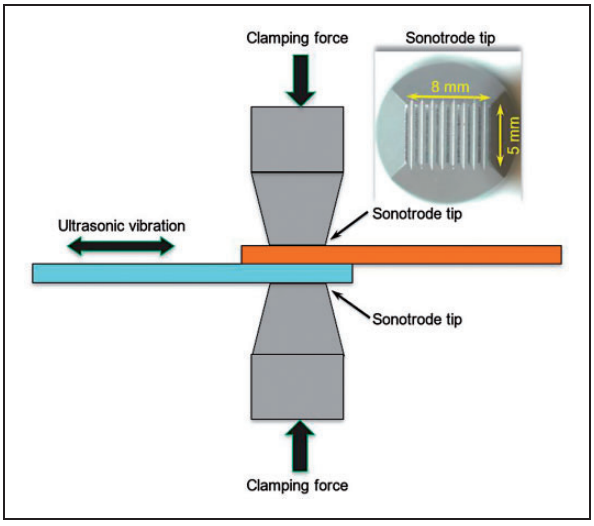

Figure 1. Schematic diagram of USW process with an image of sonotrode tip with respect to the ultrasonic vibration direction.

Results and discussion

Microstructure

Figure 2(a), (c), and (f) shows the cross-sectional micrographs of the USWed 2024-to-SiCp/2009 Al dissimilar joints produced at a welding energy of 1000, 2000, and 3000 J, respectively. No defects such as a porosity or cluster of SiC particles were observed in the dissimilar joints, indicating that the sound joints were achieved between the 2024 and SiCp/2009 Al alloys via USW. It is seen that the penetration of sonotrode (a welding tip of $5 \times 8\,mm^2$) tooth impression increased as the welding energy increased along with the thinning of both welded sheets. This happened because the higher welding energy led to increasingly higher temperatures, and the resulting softer Al sheet experienced a greater level of penetration in the weld zone compared to the base metal region. A magnified image of Figure 2(a), indicated as a Figure 2(b), shows a clear boundary between 2024 and SiCp/2009 Al alloys, which means that intermixing or diffusion between these two sides did not extensively occur due to the lack of sufficient temperature or welding energy. It is further seen from the upper part of Figure 2(b) that the SiCp particles were homogeneously distributed in the 2009 Al matrix. Figure 2(d) and (e), magnified images of

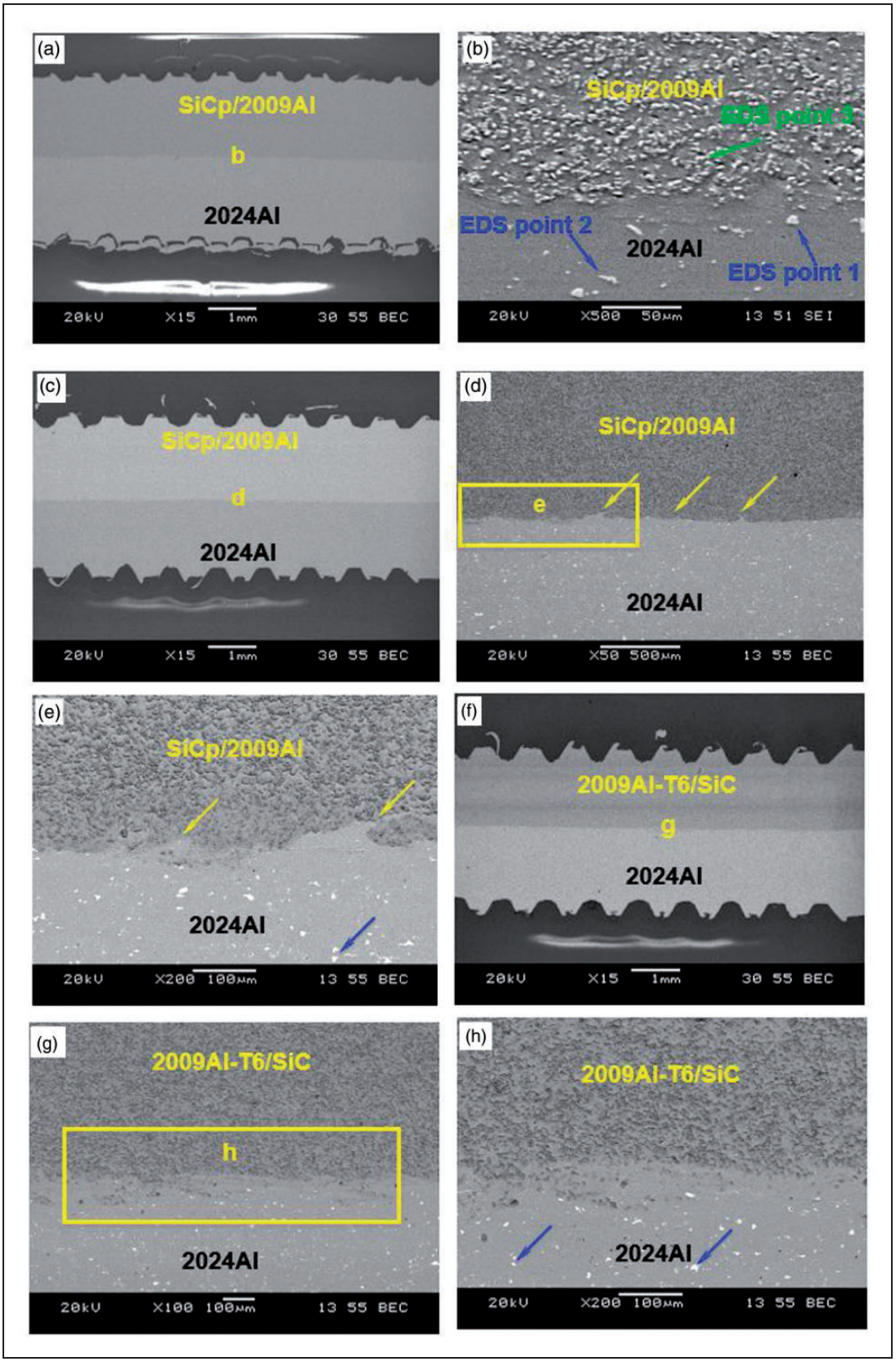

Figure 2. SEM micrographs of the USWed 2024Al-to-SiCp/2009Al dissimilar joints at a welding energy of (a, b) 1000 J, (c–e) 2000 J, and (f–h) 3000 J, respectively.

Figure 2(c), show the onset of intermixing or interlocking between two alloys (as indicated by yellow arrows), which might be beneficial for the strength of dissimilar joints (to be discussed later). Further, it is seen from Figure 2(g) and (h) that the intermixing and diffusion between two sides occurred significantly and the migration of SiCp can be easily observed in the sample welded at 3000 J. However, the migration

of SiC particles to the other side did not occur in the linear friction welding.[18] Unlike fusion welding,[19,20] no indication of the presence of visible brittle phases (such as Al_4C_3) in the weld nugget was detected in the present study. However, X-ray diffraction (XRD) will reveal more information later.

The blue arrows shown in Figure 2(b), (e), and (h) represent the particles of Al_2Cu, which were identified by energy-dispersive X-ray spectroscopy (EDS). The EDS point analysis of point 1 and point 2 showed 74.2 Al, 16.2 Cu, 6.3 Fe, and 3.3 Mn (in at.%) and 72.93 Al, 17.9 Cu, 5.0 Fe, and 4.2 Mn (in at.%), respectively. The EDS point analysis of point 3 clearly indicated the presence of SiC particles as the chemical composition showed 82.4 Al and 17.6 Si (in at.%). Our previous study[17] has also shown the generation of shear band-like structure in the similar joints of USWed SiCp/2009 composites due to the crushing of SiC particles in an intense action of abrasion during USW. However, this phenomenon was not observed in the present dissimilar welding. This could be because of SiCp only scraping against Al matrix of 2024 Al alloy rather than SiCp particles themselves in our previous study.

X-ray diffraction

To further verify the above microstructural observations, XRD patterns obtained on the matching fracture surfaces of the dissimilar USWed joints made at 1000 J and 2000 J after the tensile lap shear tests are shown in Figure 3(a) and (b), respectively. The peaks of Al_2Cu (θ) intermetallic phase appeared on both fracture surfaces of samples. This is in agreement with the SEM/EDS point analysis shown in Figure 2(b), (e), and (h). The θ phase along with G-P zones was present in T6 state and also precipitated in subsequent aging.[21] Very small peaks of SiC could be identified on the fracture surface of 2024 Al side sample of 1000 J. However, after further increasing energy to 2000 J, all peaks of SiC were intensified as shown in Figure 3(b). This is in agreement with the SEM observations shown in Figure 2, where the diffusion and intermixing between two sheets occurred extensively as the welding energy increased. It is worth mentioning that other intermetallic phases such as an Al–C phase was not observed. Thus, unlike fusion welding the frictional heat generated during USW did not promote extensive reaction between the Al matrix and SiC particles; however, this could be beyond the detection limits of XRD. According to the study by Storjohann et al.,[22] the microhardness was higher in the fusion zone in the presence of coarse Al_4C_3 needle-shaped phase. Therefore, in the following section microhardness tests were conducted in the entire welded region.

Microhardness

Three microhardness profiles diagonally across the center of the welded joints along the dotted line in the inset are shown in Figure 4. The zero point denotes the center of the NZ and the distance from the zero indicates the interval from the tested point to the center of the nugget. In the similar 2024Al-to-2024Al and SiCp/2009Al-to-SiCp/2009Al welded joints, both specimens displayed almost a constant microhardness value of 130 HV and 165 HV, respectively, throughout the weld center and base materials. Likewise, in the dissimilar welded joint of 2024Al-to-SiCp/2009Al, the microhardness values were also equivalent on their respective side. Xiao et al.[11] studied FSW of SiCp/Al and 2024Al alloys and showed that the microhardness dropped dramatically at the HAZ of 2024Al and SiCp/2009Al side due to the coarsening and dissolution of the strengthening

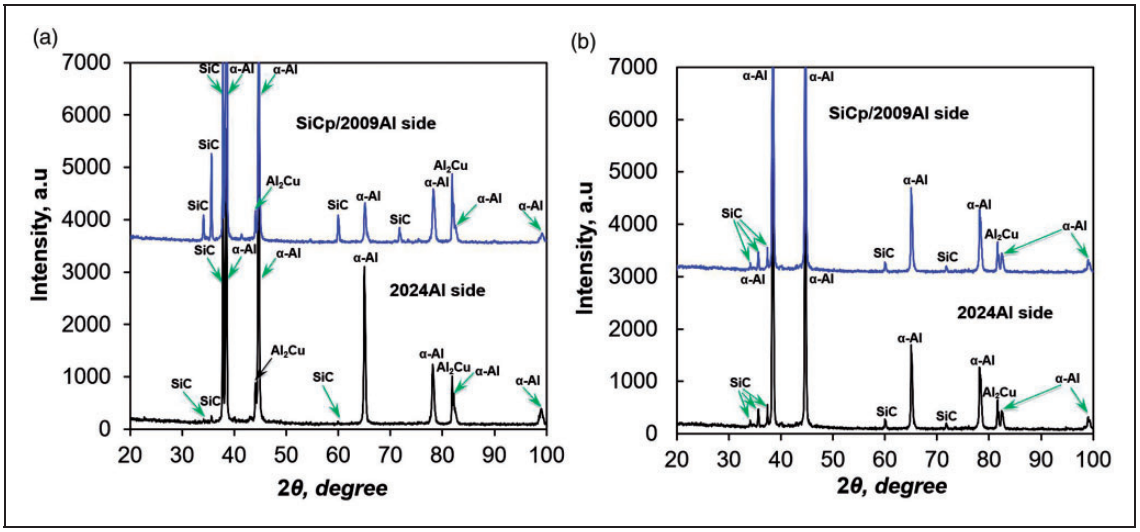

Figure 3. XRD patterns obtained from the matching fracture surfaces of both 2024Al and SiC/2009Al sides at (a) 1000 J and (b) 2000 J.

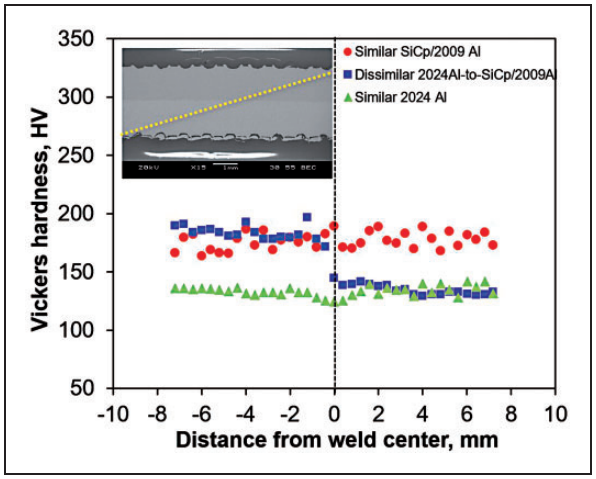

Figure 4. Microhardness profiles across the joints welded at a welding energy of 2000 J.

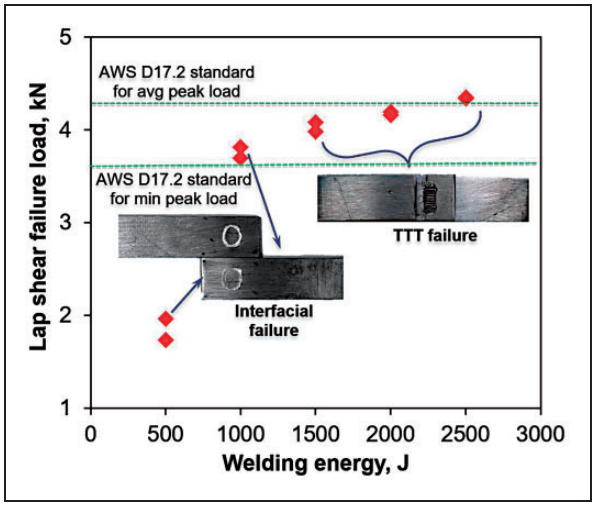

Figure 5. Tensile lap shear failure load of the USWed 2024Al-to-SiCp/2009Al dissimilar joints as a function of welding energy. TTT: transverse through thickness.

precipitates, whereas the microhardness of the NZ was lower than that of the BM due to the dissolution of the precipitates as well. However, the joints produced via the USW in the present study did not display any microhardness reduction across the entire sample due to the generation of only localized heat during welding.

Lap shear tensile fracture load

As shown in Figure 5, the tensile lap shear failure load of the USWed 2024Al-to-SiCp/2009Al dissimilar joints increased with increasing welding energy from 500 J up to 2500 J, at which the tensile lap shear failure load reached 4.3 kN. Since the AWS standard of tensile lap shear load for USW has not yet been established, AWS standard of RSW (AWS D17.2)[23] is taken as a reference, as indicated by two horizontal green lines in Figure 5. It is seen that the samples welded at a welding energy of 1000 J and beyond fulfilled the requirement of AWS D17.2 standard. At the lower welding energy (500–1000 J), the temperature was not high enough to diffuse reinforced Al matrix to unreinforced Al side, then the welded joint exhibited a weaker bond and failed from the interface (Figures 2(b) and 5). On the other hand, the samples welded at 1000 J or above displayed a greater extent of localized diffusion and intermixing/interlocking (Figure 2(e) and (h)), thus leading to a higher tensile lap shear strength, which was equivalent to that of similar SiCp/2009Al-to-SiCp/2009Al joints.[17] It should be noted that when the welding energy exceeded 3000 J, the welded joints experienced a greater degree of deformation (i.e. further deeper welding tip indentation) and fractured at the edge of the nugget zone on the SiCp/2009Al side because of the lower ductility of SiCp/2009Al compared to that of 2024 Al alloy. This was due to the presence of stress concentration stemming from the abrupt change of sheet cross-sectional area at the edge of the nugget zone at high welding temperatures or high welding energy levels as discussed in Patel et al.,[17] Mirza et al.,[24] Macwan et al.,[25] and Peng et al.[26,27]

Figure 6(a) to (c) shows the typical tensile lap shear load–displacement curves of the USWed similar 2024Al-to-2024Al, similar SiCp/2009Al-to-SiCp/2009Al, and dissimilar 2024Al-to-SiCp/2009 joints made at a welding energy of 2000 J and tested at low temperature (LT) of -40 °C, room temperature (RT), and elevated temperature (HT) of 180 °C. It is seen from Figure 6(a) that the USWed 2024Al-to-2024Al similar joints showed a high tensile lap shear strength (corresponding to a failure load of 4.7 kN) at room temperature, compared with that at low and high temperatures. It was observed that the ductility of the welded joint decreased at LT, while it increased at HT. This occurred because the thermally-activated material of weldment at HT allowed more plastic deformation while it was restricted at LT. It was also attributed to dynamic recovery caused by the movement of dislocations to sub-boundaries at HT.[28] However, similar behavior was not observed in the USWed SiCp/2009Al-to-SiCp/2009Al similar joints tested at different temperatures, since the tensile lap shear curves were all overlapped each other (Figure 6(b)). This is because SiCp/2009Al alloy contained numerous fine SiC particles, which delayed the occurrence of dynamic recovery. The tensile lap shear test curves of dissimilar 2024Al-to-SiCp/2009Al joints showed a mixed characteristic, where the joints tested at HT showed somewhat more ductile behavior; however, there was no clear difference between LT and RT. Figure 6(d) shows a summary of tensile lap shear failure load for all the similar and dissimilar joints tested at different temperatures. It is clear that the USWed similar SiCp/2009Al-to-SiCp/2009Al joints were basically not affected by test temperature from -40 °C to 180 °C, while at a LT of -40 °C all

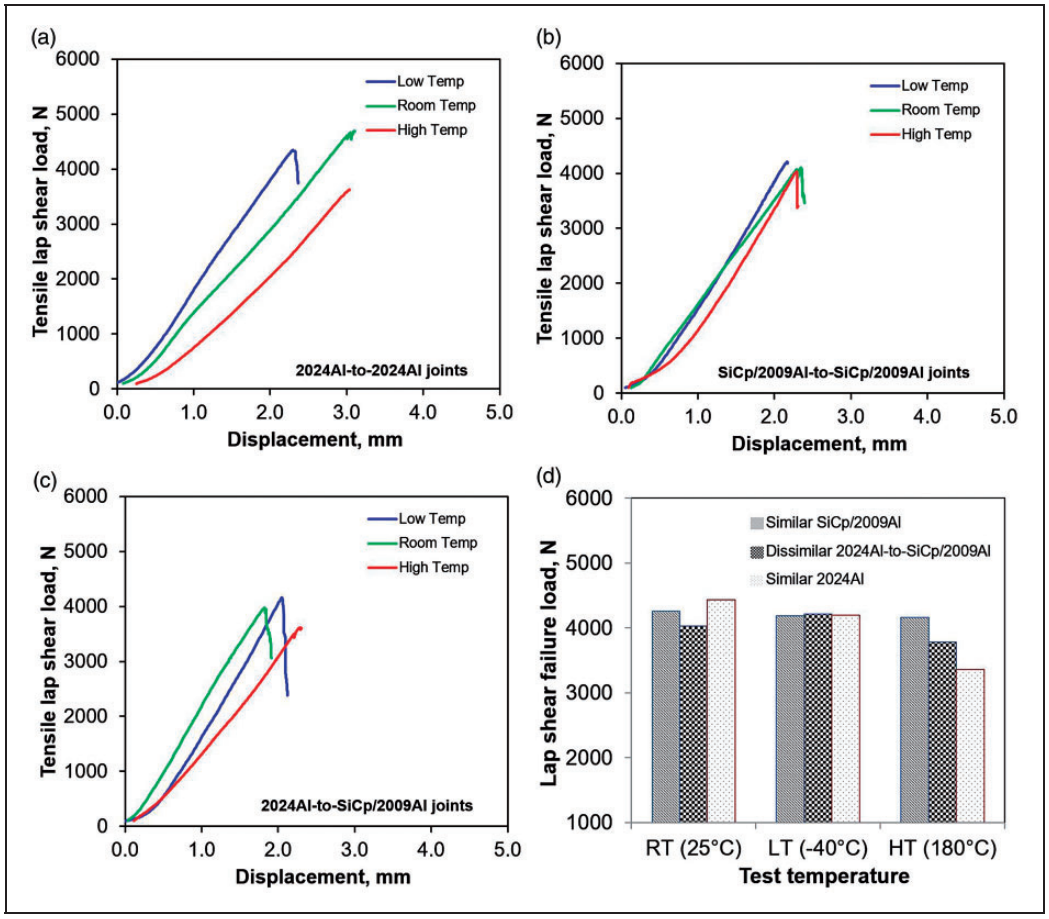

Figure 6. Typical curves of the tensile lap shear load vs. displacement of the USWed joints made at a welding energy of 2000 J. (a) Similar 2024Al-to-2024Al alloy, (b) similar SiCp/2009Al-to-SiCp/2009Al composite, and (c) dissimilar 2024Al-to-SiCp/2009Al joints tested at LT, RT, and HT, along with (d) a summary of the tensile lap shear failure loads in Figure 5(a) to (c).
LT: low temperature; RT: room temperature; HT: high temperature.

Table 1. Tensile lap shear failure locations of USWed similar 2024Al-to-2024Al alloy, similar SiCp/2009Al-to-SiCp/2009Al composite, and dissimilar 2024Al-to-SiCp/2009Al joints tested at LT, RT, and HT.

Temperature	Sample	Failure mode
Low temperature	Similar 2024Al joints	Interfacial
	Simillar SiCp/2009Al joints	TTT
	Dissimilar 2024Al-to-SiCp/2009Al joints	Interfacial
Room temperature	Similar 2024Al joints	Interfacial
	Simillar SiCp/2009Al joints	TTT
	Dissimilar 2024Al-to-SiCp/2009Al joints	TTT
High temperature	Similar 2024Al joints	Interfacial
	Simillar SiCp/2009Al joints	TTT
	Dissimilar 2024Al-to-SiCp/2009Al joints	Interfacial

TTT: transverse through thickness failure mode.

USWed joints similar tensile lap shear strength corresponding to a failure load of ~4.2 kN.

A summary about the mode of failure for different types of joints welded at a welding energy of 2000 J is shown in Table 1. It is seen that the similar 2024Al-to-2024Al joints failed along the interface at all test temperatures, while all similar joints of SiCp/2009Al-to-SiCp/2009Al composite failed at the edge of the nugget zone. This type of failure mode has been referred to as transverse through thickness (TTT) failure.[24–27,29] This happened because the higher welding energy led to a substantially higher temperature,

resulting in a greater extent of material softness and welding tip penetration. Then the sheets experienced a greater level of bending deformation in the weld zone compared with the base metal due to the outward flow of the material under the sonotrode tool indentation. This action of bending produced even a small micro-level crack at the notch of two sheets, which was observed in our previous study[30] and also in Chang et al.[31] Thus, this micro-level crack experienced a higher stress concentration effect, which allowed the crack to grow toward the outward Al sheet. As a result, the samples failed at the edge of nugget zone.

Conclusions

Defect-free dissimilar joints between SiCp/2009Al composite and 2024Al alloy were successfully achieved via USW technique. The migration of SiCp particles into the side of Al alloy along with the interlocking at the interface was observed, which increased with increasing welding energy. Unlike FSSW, USW showed a constant microhardness profile over the entire welded region, throughout the weld center and base materials. The tensile lap shear failure load of the USWed 2024Al-to-SiCp/2009Al dissimilar joints increased as the welding energy increased, and it reached ~4.5 kN, which fulfilled the requirements of AWS D17.2 standard for resistance spot welds. The tensile lap shear failure load of USWed SiCp/2009Al-to-SiCp/2009Al similar joints was nearly unchanged at different test temperatures, while the 2024Al-to-2024Al similar joints were sensitive to the test temperature to some extent. All the similar joints of 2024Al alloy tested at different temperatures failed along the interface, while all the similar joints of SiCp/2009Al composite failed in the mode of TTT crack growth due to the superior interfacial bonding along with the presence of stress concentration at the edge of nugget zone.

Acknowledgements

The assistance of Q Li, A Machin, J Amankrah, and R Churaman in performing the experiments is gratefully acknowledged.

Declaration of conflicting interests

The author(s) declared no potential conflicts of interest with respect to the research, authorship, and/or publication of this article.

Funding

The author(s) disclosed receipt of the following financial support for the research, authorship, and/or publication of this article: The authors would like to thank the Natural Sciences and Engineering Research Council of Canada (NSERC), and National Key R&D Program of China (No. 2017YFB0703104) for providing financial support, and the CAS/SAFEA International Partnership Program for Creative Research Teams led by Professor Huiming Cheng (Institute of Metal Research, Chinese Academy of Sciences). One of the authors (DL Chen) is grateful for the financial support by the Premier's Research Excellence Award (PREA), NSERC-Discovery Accelerator Supplement (DAS) Award, Canada Foundation for Innovation (CFI), and Ryerson Research Chair (RRC) program.

Note

a. According to *Science News* entitled "Air pollution kills 7 million people a year" on 25 March 2014 at http://www.sciencemag.org/news/2014/03/air-pollution-kills-7-million-people-year: "Air pollution isn't just harming Earth; it's hurting us, too. Startling new numbers released by the World Health Organization today reveal that one in eight deaths are a result of exposure to air pollution. The data reveal a strong link between the tiny particles that we breathe into our lungs and the illnesses they can lead to, including stroke, heart attack, lung cancer, and chronic obstructive pulmonary disease". And recent *Science News* entitled "Air pollution is triggering diabetes in 3.2 million people each year" on 9 July 2018 at https://www.sciencenews.org/article/air-pollution-triggering-diabetes-in-millions-each-year: "Fine particulate matter, belched out by cars and factories and generated through chemical reactions in the atmosphere, hang around as haze and make air hard to breathe. Air pollution has been linked to chronic conditions such as heart disease and diabetes (SN: 9/30/17, p.18)". The findings reveal that "air pollution [is] responsible for about 14 percent of new cases of diabetes worldwide". "The World Health Organization estimates that 422 million people now live with type 2 diabetes — up from 108 million in 1980".

ORCID iD

DL Chen http://orcid.org/0000-0003-3420-3626

References

1. Midgley G. Narrowing pathways to a sustainable future. *Science* 2018; 360: 714–715.
2. Rockström J, Gaffney O, Rogelj J, et al. A roadmap for rapid decarbonization. *Science* 2017; 355: 1269–1271.
3. Gielen D, Boshell F and Saygin D. Climate and energy challenges for materials science. *Nat Mater* 2016; 15: 117–120.
4. McNutt M. Climate change impacts. *Science* 2013; 341: 435–435.
5. Hirsch J. Recent development in aluminium for automotive applications. *Trans Nonferrous Met Soc of China* 2014; 24: 1995–2002.
6. Miller WS, Zhuang L, Bottema J, et al. Recent development in aluminium alloys for the automotive industry. *Mater Sci Eng A* 2000; 280: 37–49.
7. Bathula S, Saravanan M and Dhar A. Nanoindentation and wear characteristics of Al 5083/SiCp nanocomposites synthesized by high energy ball milling and spark plasma sintering. *J Mater Sci Technol* 2012; 28: 69–75.
8. Prasad SV and Asthana R. Aluminum metal-matrix composites for automotive applications: tribological considerations. *Tribol Lett* 2004; 17: 445–453.

9. Ni DR, Chen DL, Wang D, et al. Influence of microstructural evolution on tensile properties of friction stir welded joint of rolled SiCp/AA2009-T351 sheet. *Mater Des* 2013; 51: 199–205.
10. Wang D, Xiao BL, Wang QZ, et al. Friction stir welding of SiCp/2009Al composite plate. *Mater Des* 2013; 47: 243–247.
11. Xiao BL, Wang D, Bi J, et al. Friction stir welding of SiCp/Al composite and 2024 Al alloy. *Mater Sci Forum* 2010; 638–642: 1500–1505.
12. Salih OS, Ou H, Sun W, et al. A review of friction stir welding of aluminium matrix composites. *Mater Des* 2015; 86: 61–71.
13. Ward AA, Zhang Y and Cordero ZC. Junction growth in ultrasonic spot welding and ultrasonic additive manufacturing. *Acta Mater* 2018; 158: 393–406.
14. Ni ZL and Ye FX. Ultrasonic spot welding of aluminum alloys: a review. *J Manuf Process* 2018; 35: 580–594.
15. Gould JE. Joining aluminum sheet in the automotive industry – A 30 year history. *Weld J* 2012; 91: 23–34.
16. Patel VK, Bhole SD and Chen DL. Dissimilar ultrasonic spot welding of Mg-Al and Mg-high strength low alloy steel. *Theor Appl Mech Lett* 2014; 4-041005: 1–8.
17. Patel VK, Bhole SD, Chen DL, et al. Solid-state ultrasonic spot welding of SiCp/2009Al composite sheets. *Mater Des* 2015; 65: 489–495.
18. Rotundo F, Marconi A, Morri A, et al. Dissimilar linear friction welding between a SiC particle reinforced aluminum composite and a monolithic aluminum alloy: microstructural, tensile and fatigue properties. *Mater Sci Eng A* 2013; 559: 852–860.
19. Bassani P, Capello E, Colombo D, et al. Effect of process parameters on bead properties of A359/SiC MMCs welded by laser. *Compos Part A: Appl Sci Manuf* 2007; 38: 1089–1098.
20. Fan T, Zhang D, Shi Z, et al. The effect of Si upon the interfacial reaction characteristics in SiCp/Al-Si system composites during multiple- remelting. *J Mater Sci* 1999; 34: 5175–5180.
21. Zhang ZJ, Wang KF, Li JJ, et al. Investigation of interfacial layer for ultrasonic spot welded aluminum to copper joints. *Sci Rep* 2017; 7: Article number 12505.
22. Storjohann D, Babu SS, David SA, et al. Friction stir welding of aluminum metal matrix composites. In: *4th international symposium on friction stir welding*, Utah, USA, 2003.
23. AWS D 17.2. *Specification for resistance welding for aerospace applications*. Miami, FL: American Welding Society, 2007.
24. Mirza FA, Macwan A, Bhole SD, et al. Microstructure, tensile and fatigue properties of ultrasonic spot welded aluminum to galvanized high-strength-low-alloy and low-carbon steel sheets. *Mater Sci Eng A* 2017; 690: 323–336.
25. Macwan A, Kumar A and Chen DL. Ultrasonic spot welded 6111-T4 aluminum alloy to galvanized high-strength low-alloy steel: microstructure and mechanical properties. *Mater Des* 2017; 113: 284–296.
26. Peng H, Chen DL and Jiang XQ. Microstructure and mechanical properties of an ultrasonic spot welded aluminum alloy: effect of welding energy. *Materials* 2017; 10: 449.
27. Peng H, Jiang XQ, Bai XF, et al. Microstructure and mechanical properties of ultrasonic spot welded Mg/Al alloy dissimilar joints. *Metals* 2018; 8: 229.
28. Zacharia T and Aidun DK. Elevated temperature mechanical properties of Al-Li-Cu-Mg alloy. *Weld Res Suppl* 1988; 67: 281–288.
29. Patel VK, Bhole SD and Chen DL. Fatigue life estimation of ultrasonic spot welded Mg alloy joints. *Mater Des* 2014; 62: 124–132.
30. Patel VK, Bhole SD and Chen DL. Ultrasonic spot welded AZ31 magnesium alloy: microstructure, texture, and lap shear strength. *Mater Sci Eng A* 2013; 569: 78–85.
31. Chang B, Shi Y and Liu L. Studies on the stress distribution and fatigue behavior of weld-bonded lap shear joints. *J Mater Process Technol* 2001; 108: 307–313.